Weak localization in graphene

Vladimir I. Fal'ko [a], K. Kechedzhi [a], E. McCann [a], B. L. Altshuler [b], H. Suzuura [c], and T. Ando [d]

[a] *Department of Physics, Lancaster University, Lancaster, LA1 4YB, UK*
[b] *Physics Department, Columbia University, 538 West 120th Street, New York, NY 10027*
[c] *Division of Applied Physics, Graduate School of Engineering, Hokkaido University, Sapporo 060-8628, Japan*
[d] *Department of Physics, Tokyo Institute of Technology, 2-12-1 Ookayama, Meguro-ku, Tokyo 152-8551, Japan*

Abstract

We review the recently-developed theory of weak localization in monolayer and bilayer graphene. For high-density monolayer graphene and for any-density bilayers, the dominant factor affecting weak localization properties is trigonal warping of graphene bands, which reflects asymmetry of the carrier dispersion with respect to the center of the corresponding valley. The suppression of weak localization by trigonal warping is accompanied by a similar effect caused by random-bond disorder (due to bending of a graphene sheet) and by dislocation/antidislocation pairs. As a result, weak localization in graphene can be observed only in samples with sufficiently strong inter-valley scattering, which is reflected by a characteristic form of negative magnetoresistance in graphene-based structures.

Key words: A. Disordered systems, D. Electronic transport, D. Quantum localization
PACS: 21.55.Ak, 72.15.Rn, 73.20.Dx, 73.20.Fz

1. Introduction

The chiral nature of quasiparticles in ultra-thin graphitic films [1–5] recently revealed in quantum Hall effect measurements [6–9] originates from the honeycomb lattice structure of a monolayer of graphite (graphene). Based on the sublattice composition of electronic Bloch states and the band structure, charge carriers in monolayer and bilayer graphene have been attributed Berry phases π [1–4], and 2π [5], respectively. On the basis of the Berry phase analysis [4,10], disordered monolayer graphene can be expected to display typically weak anti-localization behavior [10,11] (similar to that in materials with strong spin-orbit coupling [12]), in contrast to bilayer graphene where one would naïvely assume the standard weak localization (WL) effect and negative magnetoresistance (MR) [13].

However, the interference properties of graphene are strongly affected [14,15] by subtle details of electronic band structure and are so sensitive to the symmetry of internal disorder [14–17] that the naïve expectations above are altered. In the absence of intervalley scattering, neither of these two materials would display any (negative or positive) WL MR. In high-density monolayers and bilayers of any density, this is due to trigonal warping of the band structure [14,15,5]. In low-density monolayer graphene, the same effect is caused by weak random-bond disorder due to bending of a graphene sheet (ripples [16]) and by dislocation/antidislocation pairs [18,17] which, from the point of view of an electron propagating in a fixed valley state, is equivalent to the effect of a random gauge field in the Dirac fermion problem [19]. The cumulative effect of all these factors can be described using the relaxation rate τ_*^{-1}, which we introduce formally in Eqs. (9) and (18) in Sections 2 and 3, respectively. However, due to the actual time-inversion symmetry of graphene, intervalley scattering restores the WL effect, so that the tendency of electrons in an infinite graphene sheet is to localize [14,20–22]. As a result, for realistic structures with a finite intervalley scattering rate, $\tau_{\rm i}^{-1} \ll \tau_*^{-1}$, Eqs. (8,17), and long enough phase-coherence time $\tau_\varphi > \tau_{\rm i}$, it is natural to display WL MR $\delta\rho(B)$ saturated at a magnetic field scale $B \sim B_{\rm i} = \frac{\hbar c}{4De}\tau_{\rm i}^{-1}$, where D is the diffusion coefficient.

Typical magnetoresistance behavior of monolayer and bilayer graphene is sketched in Fig. 1(a) and (b). The two curves in each plot illustrate two extremes: $\tau_*^{-1} \ll \tau_{\rm i}^{-1}$ and $\tau_*^{-1} \gg \tau_{\rm i}^{-1}$. In the experimentally plausible situation $\tau_*^{-1} \gg \tau_{\rm i}^{-1}$, the magnetoresistance in both mono- and bilayer material is typically of a WL type, with almost no sign of antilocalization up to the highest fields, which shows that, unlike in a ballistic regime [23] or a quan-

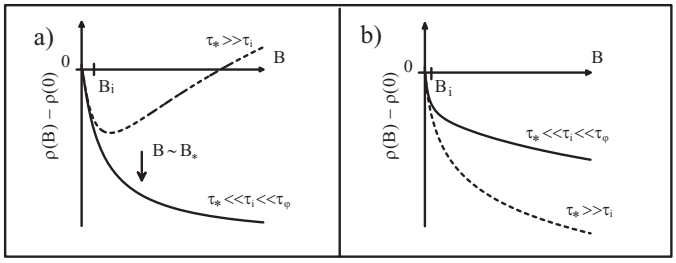

Fig. 1. (**a**) Typical magnetoresistance behavior expected in a phase–coherent ($\tau_\varphi \gg \tau_i$) monolayer of graphene for a weak intervalley scattering, $\tau_* \ll \tau_i$ (solid line) and for the case when the symmetry-breaking intravalley scattering is slower than the intervalley one $\tau_* \gg \tau_i$ (dashed). In both cases, we assume that the phase coherence time determines the longest relaxation time scale in the system. (**b**) Magnetoresistance of bilayer graphene, $\tau_* \ll \tau_i$ (solid line) and $\tau_* \gg \tau_i$ (dashed). Note that, for the case when $\tau_\varphi \ll \tau_i$ and $\tau_* \ll \tau_i$, $\Delta\rho(B) = 0$ in both monolayer and bilayer graphene.

tizing magnetic field [3,5], the chiral nature of quasiparticles does not manifest itself in the weak field magnetoresistance of realistic disordered graphene. In a hypothetical case of $\tau_*^{-1} \ll \tau_i^{-1}, \tau_\varphi^{-1}$, the magnetoresistance of monolayer graphene $\delta\rho(B)$ might change its sign at the field B_i such that $\tau_B \sim \tau_i$: from negative at $B < B_i$ to positive at higher fields, whereas in bilayer graphene with $\tau_*^{-1} \ll \tau_i^{-1}$ a longer negative WL MR tail is expected. In the regime of $\tau_\varphi^{-1} > \tau_i^{-1}$ we do not expect graphene to display any weak localization effect at all: $\Delta\rho = 0$.

Below we present a detailed analysis of the WL effect in monolayers and bilayers in Sections 2 and 3, respectively. In Section 4 we describe the effect of edges on WL in graphene and show that graphene nanoribbons should display the usual WL behavior.

2. Weak localization magnetoresistance in disordered monolayer graphene

The hexagonal lattice of monolayer graphene contains two non-equivalent sites A and B in the unit cell, as shown in Fig. 2(a). The Fermi level in neutral graphene is pinned near the corners $\mathbf{K}_\pm$ [24] of the hexagonal Brillouin zone, where the quasiparticle spectrum can be described by the Hamiltonian [1,4,14,25],

$$\hat{H}_1 = v\Pi_z\left(\sigma_x p_x + \sigma_y p_y\right) + \hat{h}_{1w} + \hat{V}_{\rm dis}, \qquad (1)$$
$$\hat{h}_{1w} = \mu\Pi_0\left[\sigma_y\left(p_x p_y + p_y p_x\right) - \sigma_x\left(p_x^2 - p_y^2\right)\right].$$

This Hamiltonian operates in the space of four-component wave functions, $\Phi = [\phi_{\mathbf{K}_+}(A), \phi_{\mathbf{K}_+}(B), \phi_{\mathbf{K}_-}(B), \phi_{\mathbf{K}_-}(A)]$ describing electronic amplitudes on A and B sites and in the valleys $\mathbf{K}_\pm$. Here, we use a direct product of AB lattice space matrices $\sigma_0 \equiv \hat{1}, \sigma_{x,y,z}$ and inter/intra-valley matrices $\Pi_0 \equiv \hat{1}, \Pi_{x,y,z}$ to highlight the difference between the form of $\hat{H}_1$ in the non-equivalent valleys. The Hamiltonian $\hat{H}_1$ takes into account nearest neighbor A/B hopping in the plane with the first (second) term representing the first (second) order term in an expansion with respect to momentum $\mathbf{p}$ measured from $\mathbf{K}_+$ and $\mathbf{K}_-$.

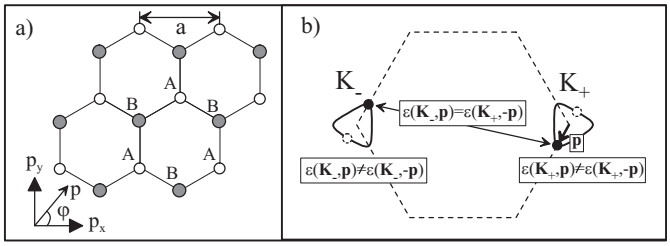

Fig. 2. (**a**)Schematic plan view of the monolayer lattice containing two sites in the unit cell, A (white circles) and B (grey), arranged on an hexagonal lattice (solid lines). (**b**)Fermi lines (solid lines) in the vicinity of two inequivalent valleys $\mathbf{K}_+$ and $\mathbf{K}_-$ of the hexagonal Brillouin zone (dashed line). Trigonal warping produces asymmetry of the dispersion at each valley $\epsilon(\mathbf{K}_\pm, \mathbf{p}) \neq \epsilon(\mathbf{K}_\pm, -\mathbf{p})$, where momentum $\mathbf{p}$ is determined with respect to the center of the valley, but the effects of warping in the valleys have opposite signs, $\epsilon(\mathbf{K}_\pm, \mathbf{p}) = \epsilon(\mathbf{K}_\mp, -\mathbf{p})$.

Near the center of the valley $\mathbf{K}_+$, the Dirac-type part, $v\,\sigma\cdot\mathbf{p}$, of $\hat{H}_1$ determines the linear dispersion $\epsilon = vp$ for the electron in the conduction band and $\epsilon = -vp$ for the valence band. Electrons in the conduction and valence bands also differ by the isospin projection onto the direction of their momentum (chirality): $\sigma\cdot\mathbf{p}/p = 1$ in the conduction band, $\sigma\cdot\mathbf{p}/p = -1$ in the valence band. In the valley $\mathbf{K}_-$, the electron chirality is mirror-reflected: it fixes $\sigma\cdot\mathbf{p}/p = -1$ for the conduction band and $\sigma\cdot\mathbf{p}/p = 1$ for the valence band. For an electron in the conduction band, the plane wave states are

$$\Phi_{\mathbf{K}_\pm,\mathbf{p}} = \frac{e^{i\mathbf{pr}/\hbar}}{\sqrt{2}}\left(e^{i\varphi/2}|\downarrow\rangle_{\mathbf{K}_\pm,\mathbf{p}} \pm e^{-i\varphi/2}|\uparrow\rangle_{\mathbf{K}_\pm,\mathbf{p}}\right), \qquad (2)$$
$$\Phi_{\mathbf{K}_\pm,-\mathbf{p}} = \frac{ie^{-i\mathbf{pr}/\hbar}}{\sqrt{2}}\left(e^{i\varphi/2}|\downarrow\rangle_{\mathbf{K}_\pm,-\mathbf{p}} \mp e^{-i\varphi/2}|\uparrow\rangle_{\mathbf{K}_\pm,-\mathbf{p}}\right)$$

Here $|\uparrow\rangle_{\mathbf{K}_+,\mathbf{p}} = [1,0,0,0]$, $|\downarrow\rangle_{\mathbf{K}_+,\mathbf{p}} = [0,1,0,0]$ and $|\uparrow\rangle_{\mathbf{K}_-,\mathbf{p}} = [0,0,1,0]$, $|\uparrow\rangle_{\mathbf{K}_-,\mathbf{p}} = [0,0,0,1]$, the factors $e^{\pm i\varphi/2}$ take into account the chirality, and $\mathbf{p} = (p\cos\varphi, p\sin\varphi)$.

The term $\hat{h}_{1w}$ in Eq. (1) leads to a trigonal deformation of a single-connected Fermi line and $\mathbf{p} \to -\mathbf{p}$ asymmetry of the electron dispersion inside each valley, as illustrated in Fig. 2(b): $\epsilon(\mathbf{K}_\pm, \mathbf{p}) \neq \epsilon(\mathbf{K}_\pm, -\mathbf{p})$. However, due to time-reversal symmetry [26] trigonal warping has opposite signs in the two valleys and $\epsilon(\mathbf{K}_\pm, \mathbf{p}) = \epsilon(\mathbf{K}_\mp, -\mathbf{p})$.

The interplay between the two terms in $\hat{H}_1$ resulting in the asymmetry of the electronic dispersion manifests itself in the WL behavior. The WL correction to conductivity in disordered conductors is a result of the constructive interference of electrons propagating around closed loops in opposite directions [13] as sketched in Fig. 3(b).

WL is usually described [13] in terms of the particle-particle correlation function, Cooperon. Following the example of Cooperons for a spin $\frac{1}{2}$, we classify Cooperons as singlets and triplets in terms of 'isospin' (AB lattice space) and 'pseudospin' (inter/intra-valley) indices. In fact, with regards to the isospin (sublattice) composition of Cooperons in a disordered monolayer, only singlet modes are rel-

evant. This is because a correlator describing two plane waves, $\Phi_{\mathbf{K}_+,\mathbf{p}}$ and $\Phi_{\mathbf{K}_-,-\mathbf{p}}$ Eq. (2), propagating in opposite directions along a ballistic segment of a closed trajectory as in Fig. 3(b) has the following form:

$$\Phi_{\mathbf{K},\mathbf{p}}\Phi_{\mathbf{K}',-\mathbf{p}} \sim |\uparrow\rangle_{\mathbf{K},\mathbf{p}}|\downarrow\rangle_{\mathbf{K}',-\mathbf{p}} - |\downarrow\rangle_{\mathbf{K},\mathbf{p}}|\uparrow\rangle_{\mathbf{K}',-\mathbf{p}} - e^{-i\varphi}|\uparrow\rangle_{\mathbf{K},\mathbf{p}}|\uparrow\rangle_{\mathbf{K}',-\mathbf{p}} + e^{i\varphi}|\downarrow\rangle_{\mathbf{K},\mathbf{p}}|\downarrow\rangle_{\mathbf{K}',-\mathbf{p}}.$$

It contains only sublattice-singlet terms (the first two terms) because triplet terms (the last two terms) disappear after averaging over the direction of momentum, $\mathbf{p} = (p\cos\varphi, p\sin\varphi)$, so that $\langle e^{\pm i\varphi}\rangle_\varphi = 0$. In fact, our diagrammatic calculation [14] shows that the interference correction to the conductivity of graphene is determined by the interplay of four isospin singlet modes: one pseudospin singlet and three pseudospin triplets. Of these, two of the pseudospin triplet modes are intravalley Cooperons while the remaining triplet and the singlet are intervalley Cooperons.

In the WL picture for a diffusive electron in a metal, two phases ϑ_1 and ϑ_2 acquired while propagating along paths "1" and "2" [see Fig. 3(b)] are exactly equal, so that the interference of such paths is constructive and, as a result, enhances backscattering leading to WL [13]. In monolayer graphene the Berry phase π characteristic for quasiparticles described by the first term of $\hat{H}_1$, determines the phase difference $\delta \equiv \vartheta_1 - \vartheta_2 = \pi N$ (where N is the winding number of a trajectory) [10,14], and one would expect weak anti-localization behavior. However, the asymmetry of the electron dispersion due to $\hat{h}_{1\mathrm{w}}$, leading to warping of the Fermi line around each valley as in Fig. 2, deviates δ from πN. Indeed, any closed trajectory is a combination of ballistic intervals, Fig. 3(b). Each interval, characterized by the momenta $\pm\mathbf{p_j}$ (for the two directions) and by its duration t_j, contributes to the phase difference $\delta_j = [\epsilon(\mathbf{p_j}) - \epsilon(-\mathbf{p_j})]t_j = \hat{h}_{1\mathrm{w}}(\mathbf{p_j})t_j$. Since δ_j are random uncorrelated, the mean square of $\delta = \sum\delta_j$ can be estimated as $\langle\delta^2\rangle \sim \langle(t_j\hat{h}_{1\mathrm{w}}(\mathbf{p_j}))^2\rangle t/\tau_{tr}$, where t is the duration of the path and τ_{tr} is the transport mean free time [27].

Warping thus determines the relaxation rate,

$$\tau_{\mathrm{w}}^{-1} \approx \tau_0\langle \mathrm{Tr}\hat{h}_{1\mathrm{w}}^2(\mathbf{p})\rangle_\varphi/(2\hbar^2) \approx 2\tau_0\left(\epsilon^2\mu/\hbar v^2\right)^2, \qquad (3)$$

which suppresses intravalley Cooperons, and, thus, weak anti-localization in the case when electrons seldom change their valley state. The two intervalley Cooperons are not affected by trigonal warping due to time-reversal symmetry of the system which requires $\epsilon(\mathbf{K}_\pm,\mathbf{p}) = \epsilon(\mathbf{K}_\mp,-\mathbf{p})$, Fig. 2. These two Cooperons cancel each other in the case of weak intervalley scattering, thus giving $\delta g \sim 0$. However, intervalley scattering, with rate τ_{i}^{-1} larger than the decoherence rate τ_φ^{-1}, breaks their exact cancellation and partially restores weak localization.

To describe the valley symmetry of monolayer graphene and parameterize all possible types of disorder, we introduce two sets of 4×4 Hermitian matrices the 'isospin' matrices $\vec{\Sigma} = (\Sigma_x, \Sigma_y, \Sigma_z)$ with $[\Sigma_{s_1}, \Sigma_{s_2}] = 2i\varepsilon^{s_1s_2s_3}\Sigma_{s_3}$, and

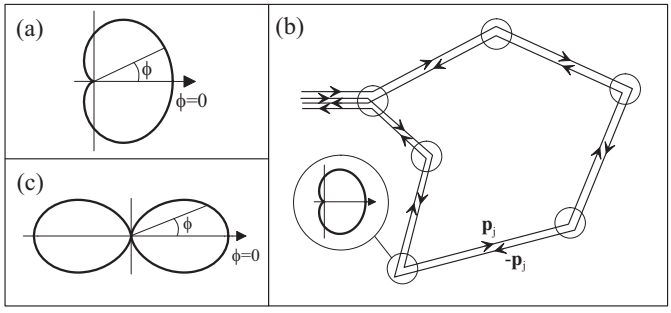

Fig. 3. (a) Angular dependence $w(\varphi) \sim \cos^2(\varphi/2)$ of the scattering probability off an $A-B$ symmetric potential $Iu(\mathbf{r})$ in monolayer graphene. It demonstrates the fact that the chiral states Eq. (2) with isospin fixed to the direction of momentum display an absence of back scattering [4,10], leading to a transport time longer than the scattering time $\tau_{\mathrm{tr}} = 2\tau_0$. (b) A pair of closed paths which contribute to weak localization, (c) Angular dependence $w(\varphi) \sim \cos^2(\varphi)$ of the scattering probability off an $A-B$ symmetric potential in bilayer graphene, which determines coinciding transport and scattering times.

'pseudospin' matrices $\vec{\Lambda} = (\Lambda_x, \Lambda_y, \Lambda_z)$ with $[\Lambda_{l_1}, \Lambda_{l_2}] = 2i\varepsilon^{l_1l_2l_3}\Sigma_{l_3}$, defined as

$$\Sigma_x = \Pi_z\otimes\sigma_x,\ \Sigma_y = \Pi_z\otimes\sigma_y,\ \Sigma_z = \Pi_0\otimes\sigma_z, \qquad (4)$$

$$\Lambda_x = \Pi_x\otimes\sigma_z,\ \Lambda_y = \Pi_y\otimes\sigma_z,\ \Lambda_z = \Pi_z\otimes\sigma_0. \qquad (5)$$

The operators $\vec{\Sigma}$ and $\vec{\Lambda}$ form two mutually independent algebras equivalent to the algebra of Pauli matrices (in Eqs. (4,5) $\varepsilon^{s_1s_2s_3}$ is the antisymmetric tensor and $[\Sigma_s, \Lambda_l] = 0$) thus they determine two commuting subgroups of the group U_4 of unitary transformations [28] of a 4-component Φ: an 'isospin' sublattice group $\mathrm{SU}_2^\Sigma \equiv \{e^{ia\vec{n}\vec{\Sigma}}\}$ and a 'pseudospin' valley group $\mathrm{SU}_2^\Lambda \equiv \{\mathrm{e}^{ib\vec{n}\cdot\vec{\Lambda}}\}$. Also, $\vec{\Sigma}$ and $\vec{\Lambda}$ change sign under the inversion of time, whereas products $\Sigma_s\Lambda_l$ are $t\to -t$ invariant [26] and can be used as a basis for a quantitative phenomenological description of non-magnetic static disorder [29,30].

The operators $\vec{\Sigma}$ and $\vec{\Lambda}$ help us to represent the electron Hamiltonian in weakly disordered graphene as

$$\hat{H}_1 = v\,\vec{\Sigma}\mathbf{p} + \hat{h}_{1\mathrm{w}} + \hat{\mathrm{I}}u(\mathbf{r}) + \sum_{s,l=x,y,x}\Sigma_s\Lambda_l u_{s,l}(\mathbf{r}), \qquad (6)$$

$$\text{where}\ \ \hat{h}_{1\mathrm{w}} = -\mu\Sigma_x(\vec{\Sigma}\mathbf{p})\Lambda_z\Sigma_x(\vec{\Sigma}\mathbf{p})\Sigma_x.$$

The Dirac-type part $v\,\vec{\Sigma}\mathbf{p}$ of $\hat{H}_1$ in Eq.(6) and potential disorder $\hat{\mathrm{I}}u(\mathbf{r})$ (where $\hat{\mathrm{I}}$ is a 4×4 unit matrix and $\langle u(\mathbf{r})\,u(\mathbf{r}')\rangle = u^2\delta(\mathbf{r}-\mathbf{r}')$) do not contain valley operators Λ_l, thus, they remain invariant with respect to the pseudospin transformations from valley group SU_2^Λ. If disorder due to charges lying in a substrate at distances from the graphene sheet shorter or comparable to the electron wavelength h/p_{F} dominates the elastic scattering rate, then $\tau^{-1} \approx \tau_0^{-1} = \pi\gamma u^2/\hbar$, where $\gamma = p_{\mathrm{F}}/(2\pi\hbar^2 v)$ is the density of states of quasiparticles per spin in one valley.

All other types of disorder, which break the SU_2^Λ pseudospin symmetry of the system, are included in a random matrix $\Sigma_s\Lambda_l u_{s,l}(\mathbf{r})$. In particular, $u_{z,z}(\mathbf{r})$ describes differ-

ent on-site energies on the A and B sublattices, caused by atomically sharp defects. Terms with $u_{x(y),z}(\mathbf{r})$ play the role of a valley-antisymmetric vector potential. Such disorder [19] naturally appears in honeycomb lattice models with random bonds [30], which can be used to model randomly bent graphene sheets [16] and graphene with a finite concentration of dislocation/antidislocation pairs [18,17]. Terms with $u_{s,x(y)}(\mathbf{r})$ take into account inter-valley scattering. For simplicity, we assume that different types of disorder are uncorrelated, $\langle u_{s,l}(\mathbf{r})u_{s',l'}(\mathbf{r}')\rangle = u_{sl}^2\delta_{ss'}\delta_{ll'}\delta(\mathbf{r}-\mathbf{r}')$ and, on average, isotropic in the $x-y$ plane, $u_{xl}^2 = u_{yl}^2 \equiv u_{\perp l}^2$, $u_{sx}^2 = u_{sy}^2 \equiv u_{s\perp}^2$. We parameterize them by scattering rates $\tau_{sl}^{-1} = \pi\gamma u_{sl}^2/\hbar$. Also, the warping term, $\hat{h}_{1\mathrm{w}}$ lifts the pseudospin symmetry SU_2^{Λ}, though it remains invariant under pseudospin rotations around the z-axis.

In the formal WL analysis, we use a Cooperon matrix $C_{\alpha\beta\alpha'\beta'}^{\xi\mu\xi'\mu'}$ where subscripts describe the isospin state of incoming $\alpha\beta$ and outgoing $\alpha'\beta'$ pairs of electrons and superscripts describe the pseudospin state of incoming $\xi\mu$ and outgoing $\xi'\mu'$ pairs. We classify Cooperons as singlets and triplets in terms of isospin and pseudospin indices $C_{S_1S_2}^{M_1M_2}$. For example, $M=0$ is a 'pseudospin-singlet', $M=x,y,z$ are three 'pseudospin-triplet' components; $S=0$ is an 'isospin-singlet' and $S=x,y,z$ are 'isospin-triplet' components [31].

It turns out [14] that the WL correction to the conductivity in terms of Cooperons reads [32]

$$\delta g = \frac{2e^2D}{\pi\hbar}\int\frac{d^2q}{(2\pi)^2}\left(C_0^x + C_0^y + C_0^z - C_0^0\right). \qquad (7)$$

The last term in Eq. (7), C_0^0 is the only true gapless mode which determines the dominance of the WL sign in the quantum correction to the conductivity in graphene with a long phase coherence time, $\tau_\varphi > \tau_{\mathrm{i}}$. Amongst the rest, the intervalley component C_0^z has a gap $2\tau_{\mathrm{i}}^{-1}$ determined by the intervalley scattering rate,

$$\tau_{\mathrm{i}}^{-1} = 4\tau_{\perp\perp}^{-1} + 2\tau_{z\perp}^{-1}, \qquad (8)$$

two intravalley components C_0^x, C_0^y have gaps τ_*^{-1} determined by cumulative inter/intra valley scattering rates which also include the trigonal warping effect,

$$\tau_*^{-1} \equiv \tau_{\mathrm{w}}^{-1} + 2\tau_{\mathrm{z}}^{-1} + \tau_{\mathrm{i}}^{-1}, \text{ where } \tau_{\mathrm{z}}^{-1} = 2\tau_{\perp z}^{-1} + \tau_{zz}^{-1}. \qquad (9)$$

Here we use the $x-y$ plane isotropy of disorder, $\tau_{sx}^{-1} = \tau_{sy}^{-1} \equiv \tau_{s\perp}^{-1}$ and $\tau_{xl}^{-1} = \tau_{yl}^{-1} \equiv \tau_{\perp l}^{-1}$.

Using expression Eq. (7), we find the $B=0$ temperature dependent correction, $\delta\rho/\rho = -\delta g/g$, to the graphene sheet resistance. Taking into account the double spin degeneracy of carriers we present

$$\frac{\delta\rho\,(0)}{\rho^2} = \frac{e^2}{\pi h}\ln(1+2\frac{\tau_\varphi}{\tau_{\mathrm{i}}}) + \delta_0, \qquad (10)$$

and evaluate magnetoresistance, $\rho(B)-\rho(0) \equiv \Delta\rho(B)$,

$$\Delta\rho(B) = -\frac{e^2\rho^2}{\pi h}\left[F(\frac{B}{B_\varphi}) - F(\frac{B}{B_\varphi + 2B_{\mathrm{i}}})\right] + \delta(B), \qquad (11)$$

$$F(z) = \ln z + \psi(\frac{1}{2}+\frac{1}{z}),\ B_{\varphi,\mathrm{i},*} = \frac{\hbar c}{4De}\tau_{\varphi,\mathrm{i},*}^{-1}.$$

The latter result is sketched in Fig. 1. Here, ψ is the digamma function and the decoherence (taken into account by the rate τ_φ^{-1}) determines the curvature of the magnetoresistance at $B < B_\varphi \equiv \hbar c/4De\tau_\varphi$. The small corrections $\delta_0 = -[2e^2/(\pi h)]\ln\frac{\tau_\varphi/\tau_{\mathrm{tr}}}{1+\tau_\varphi/\tau_*}$ and $\delta(B) = [2e^2\rho^2/(\pi h)]F(\frac{B}{B_\varphi+B_*})$ originate from two intravalley Cooperons strongly suppressed by the trigonal warping effect and intravalley scattering. For $B_* \gg B_{\mathrm{i}}$, the MR $\Delta\rho(B)$ is distinctly of a WL type, with almost no sign of antilocalization. Such behavior is expected in graphene tightly coupled to an insulating substrate (which generates atomically sharp scatterers). In a sheet loosely attached to a substrate (or suspended), the intervalley scattering time may be longer than the decoherence time, $\tau_{\mathrm{i}} > \tau_\varphi > \tau_{\mathrm{w}}$ ($B_{\mathrm{i}} < B_\varphi < B_*$). In this case MR would display neither WL nor antilocalization behavior: $\Delta\rho(B) = 0$.

3. Bilayer graphene

Bilayer graphene consists of two coupled monolayers. Its unit cell contains four inequivalent sites, $A, B, \tilde{A}$ and $\tilde{B}$ (A, B and $\tilde{A}, \tilde{B}$ lie in the bottom and top layer, respectively) arranged according to Bernal stacking [33,5]: sites B of the honeycomb lattice in the bottom layer lie exactly below $\tilde{A}$ of the top layer. The Brillouin zone of the bilayer, similarly to the one in monolayer, has two inequivalent degeneracy points $\mathbf{K}_+$ and $\mathbf{K}_-$ which determine two valleys centered around $\epsilon = 0$ in the electron spectrum [24]. Near the center of each valley the electron spectrum consists of four branches. Two branches describing states on sublattices $\tilde{A}$ and B are split from energy $\epsilon = 0$ by about $\pm\gamma_1$, the interlayer coupling, whereas two low-energy branches are formed by states based upon sublattices A and $\tilde{B}$. The latter can be described [5] using a Hamiltonian which acts in the space of four-component wave functions $\Phi = [\phi_{\mathbf{K}_+,A}, \phi_{\mathbf{K}_+,\tilde{B}}, \phi_{\mathbf{K}_-,\tilde{B}}, \phi_{\mathbf{K}_-,A}]$, where $\phi_{\xi,\alpha}$ is an electron amplitude on the sublattice $\alpha = A, \tilde{B}$ and in the valley $\xi = \mathbf{K}_+, \mathbf{K}_-$:

$$\hat{H}_{2L} = -\frac{1}{2m}\left[\left(p_x^2 - p_y^2\right)\sigma_x + 2p_xp_y\sigma_y\right] + \hat{h}_{2\mathrm{w}} + \hat{V}, \qquad (12)$$
$$\hat{h}_{2\mathrm{w}} = v_3\Pi_z\left(p_x\sigma_x - p_y\sigma_y\right).$$

Here, $\sigma_{x,y,z}$ and $\Pi_{x,y,z}$ are Pauli matrices acting in sublattice and valley space, respectively.

The first term in Eq. (12) is the leading contribution in the nearest neighbors approximation of the tight-binding model [5]. This approximation takes into account both intralayer hopping $A \leftrightarrow B$ and $\tilde{A} \leftrightarrow \tilde{B}$ (that leads to the Dirac-type dispersion $\epsilon = \pm pv$ near the Fermi point $\mathbf{K}_\pm$ in a monolayer) and the interlayer $\tilde{A} \leftrightarrow B$ hopping. This term yields the parabolic spectrum $\epsilon = \pm p^2/2m$ with $m = \gamma_1/2v^2$ which dominates in the intermediate energy range $\frac{1}{4}\gamma_1(v_3/v)^2 < \varepsilon_F < \frac{1}{4}\gamma_1$. In this regime we can truncate the

expansion of $\hat{H}(\mathbf{p})$ in powers of the momentum $\mathbf{p}$ neglecting terms of the order higher than quadratic.

Electron waves characteristic for the first, quadratic, term of $\hat{H}_{2L}$ have the form

$$\Phi_{\mathbf{K},\pm\mathbf{p}} = \pm\frac{e^{\pm i\mathbf{px}/\hbar}}{\sqrt{2}}\left(e^{-i\varphi}|\uparrow\rangle_{\mathbf{K},\pm\mathbf{p}} - e^{i\varphi}|\downarrow\rangle_{\mathbf{K},\pm\mathbf{p}}\right), \qquad (13)$$

where $|\uparrow\rangle_{\mathbf{K}_+,\pm\mathbf{p}} = [1,0,0,0]$, $|\downarrow\rangle_{\mathbf{K}_+,\pm\mathbf{p}} = [0,1,0,0]$ and $|\uparrow\rangle_{\mathbf{K}_-,\pm\mathbf{p}} = [0,0,1,0]$, $|\uparrow\rangle_{\mathbf{K}_-,\pm\mathbf{p}} = [0,0,0,1]$. These are eigenstates of an operator $\sigma\mathbf{n}_2$ with $\sigma\mathbf{n}_2 = -1$ for electrons in the conduction band and $\sigma\mathbf{n}_2 = 1$ for electrons in the valence band, where $\mathbf{n}_2(\mathbf{p}) = (\cos(2\varphi), \sin(2\varphi))$ for $\mathbf{p} = (p\cos\varphi, p\sin\varphi)$, which means that they are chiral, but with the degree of chirality different from the one found in the monolayer (see Sec. 2).

The second term in Eq. (12), $\hat{h}_{2\mathrm{w}}$, originates from a weak direct $A \leftrightarrow \tilde{B}$ interlayer coupling. It leads to a Lifshitz transition in the shape of the Fermi line of the 2D electron gas which takes place when $\epsilon_\mathrm{F} \sim \epsilon_\mathrm{L} \equiv \frac{1}{4}\gamma_1(v_3/v)^2$ corresponding to density $n_\mathrm{L} \sim v_3^2\gamma_1^2/(2\pi\hbar^2v^4) \sim 10^{11}\mathrm{cm}^{-2}$ (using $v_3/v \sim 0.1$). In a bilayer with $\epsilon_\mathrm{F} < \epsilon_\mathrm{L}$, the interplay between the two terms in $\hat{H}_{2L}$ determines the Fermi line in the form of four pockets [5] in each valley. In a bilayer with $\epsilon_\mathrm{F} > \epsilon_\mathrm{L}$, $\hat{h}_{2\mathrm{w}}$ can be treated as a perturbation leading to a trigonal deformation of a single-connected Fermi line, thus manifesting the asymmetry of the electron dispersion inside each valley: $\epsilon(\mathbf{K}_\pm, \mathbf{p}) \neq \epsilon(\mathbf{K}_\pm, -\mathbf{p})$. This asymmetry leads to the dephasing effect of electron trajectories similar to the one discussed in the case of the monolayer, and is characterized by the scattering rate

$$\tau_\mathrm{w}^{-1} \approx \begin{cases} \frac{1}{2\hbar^2}\tau\langle\mathrm{Tr}\hat{h}_{2\mathrm{w}}^2(\mathbf{p})\rangle_\varphi \sim \pi n_L l^2\tau^{-1}, & \pi n_L l^2 < 1 \\ \tau^{-1}, & \pi n_L l^2 > 1 \end{cases}. \qquad (14)$$

We estimate that for the recently studied bilayers [9] with $n_e = 2.5\times10^{12}\mathrm{cm}^{-2}$, $l \sim 0.1\mu\mathrm{m}$ and $\tau_\mathrm{w} \sim \tau$.

The term $\hat{V}$ in Eq. (12) describes time-reversal-symmetric disorder. It is parameterized using $t \to -t$ symmetric 4×4 matrices acting in the sublattice/valley space,

$$\hat{V} = \sum_{s,l=0,x,y} \Pi_l\sigma_s u_{sl}(\mathbf{r}) + \Pi_z\sigma_z u_{zz}(\mathbf{r}). \qquad (15)$$

The sum in Eq. (15) contains valley and isospin conserving disorder potential $\hat{I}u(\mathbf{r})$, with $\langle u(\mathbf{r})u(\mathbf{r}')\rangle = u^2\delta(\mathbf{r}-\mathbf{r}')$ and $\tau_0^{-1} = \pi\gamma u^2/\hbar, \gamma = \frac{m}{2\pi}$, which originates from charged impurities in the SiO_2 substrate and is assumed to be the dominant mechanism of scattering in the system. All other types of disorder which breaks valley and sublattice symmetries are assumed to be uncorrelated, $\langle u_{s\,l}(\mathbf{r})u_{s'\,l'}(\mathbf{r}')\rangle = u_{s\,l}^2\delta_{ss'}\delta_{ll'}\delta(\mathbf{r}-\mathbf{r}')$. We characterize them using scattering rates $\tau_{s\,l}^{-1} = \pi\gamma u_{s\,l}^2/\hbar$. Furthermore, the scattering is assumed to be isotropic in the $x-y$ plane, so that $u_{xl}^2 = u_{yl}^2 \equiv u_{\perp l}^2, u_{s\,x}^2 = u_{sy}^2 \equiv u_{s\perp}^2$.

To analyze the WL effect we introduce a Cooperon matrix $C_{\alpha\beta\alpha'\beta'}^{\xi\mu\xi'\mu'}$ where subscripts describe the sublattice state of incoming $\alpha\beta$ and outgoing $\alpha'\beta'$ pairs of electrons and superscripts describe the valley state of incoming $\xi\mu$ and outgoing $\xi'\mu'$ pairs. With the bilayer Hamiltonian written in terms of Π, σ matrices Eqs. (12), we parameterize Cooperons as $C_{S_1S_2}^{M_1M_2}$ by M_1, M_2 'valley' and S_1, S_2 'sublattice' singlet and triplet states in a similar way to monolayer isospin and pseudospin states. The sublattice composition of Cooperons is determined by the correlator of plane waves propagating ballistically in opposite directions,

$$\Phi_{\mathbf{K},\mathbf{p}}\Phi_{\mathbf{K}',-\mathbf{p}} \sim |\uparrow\rangle_{\mathbf{K},\mathbf{p}}|\downarrow\rangle_{\mathbf{K}',-\mathbf{p}} + |\downarrow\rangle_{\mathbf{K},\mathbf{p}}|\uparrow\rangle_{\mathbf{K}',-\mathbf{p}} - e^{2i\varphi}|\uparrow\rangle_{\mathbf{K},\mathbf{p}}|\uparrow\rangle_{\mathbf{K}',-\mathbf{p}} - e^{-2i\varphi}|\downarrow\rangle_{\mathbf{K},\mathbf{p}}|\downarrow\rangle_{\mathbf{K}',-\mathbf{p}}.$$

After averaging over the momentum direction the terms corresponding to $C_{x,y}^M \propto (|\uparrow\rangle_{\mathbf{K},\mathbf{p}}|\uparrow\rangle_{\mathbf{K}',-\mathbf{p}} \pm |\downarrow\rangle_{\mathbf{K},\mathbf{p}}|\downarrow\rangle_{\mathbf{K}',-\mathbf{p}})$ disappear, since $\mathbf{p} = (p\cos\varphi, p\sin\varphi)$ so that $\langle e^{\pm2i\varphi}\rangle_\varphi = 0$, whereas terms corresponding to the sublattice symmetric Cooperons, $C_z^M \propto (|\uparrow\rangle_{\mathbf{K},\mathbf{p}}|\downarrow\rangle_{\mathbf{K}',-\mathbf{p}} + |\downarrow\rangle_{\mathbf{K},\mathbf{p}}|\uparrow\rangle_{\mathbf{K}',-\mathbf{p}})$ remain non-zero.

The interference correction to the conductivity in a bilayer can be expressed in terms of four components of $C(\mathbf{r},\mathbf{r})$, the Cooperon taken at coinciding coordinates, corresponding to valley singlet and three valley triplets:

$$\delta g = \frac{2e^2D}{\pi\hbar}\left[-C_z^z + C_z^0 - C_z^x - C_z^y\right]. \qquad (16)$$

The WL correction Eq. (16) is determined by the two intervalley Cooperon modes, the gapless valley-symmetric mode C_z^z and valley-asymmetric C_z^0 with the gap $2\tau_\mathrm{i}^{-1}$ determined by intervalley scattering rate,

$$\tau_\mathrm{i}^{-1} = 4\tau_{\perp\perp}^{-1} + 2\tau_{z\perp}^{-1}. \qquad (17)$$

In the absence of the intervalley scattering, the contributions of C_z^0 and C_z^z are equal in magnitude, so that they cancel, which leads to suppressed WL MR. In the case of strong intervalley scattering due to atomically sharp defects, $\tau_\mathrm{i} \ll \tau_\varphi$, this exact cancellation is broken and WL is partially restored. For completeness, in Eq. (16) we have retained the intravalley Cooperons $C_z^{x,y}$, though they have larger gaps τ_*^{-1}, and, thus, are strongly suppressed by by trigonal warping intravalley and intervalley disorder,

$$\tau_*^{-1} \equiv \tau_\mathrm{w}^{-1} + 2\tau_\mathrm{z}^{-1} + \tau_\mathrm{i}^{-1}, \quad \tau_\mathrm{z}^{-1} = 2\tau_{zz}^{-1}. \qquad (18)$$

Equation (10) yields the zero field WL correction to the resistivity and the WL MR is described by Eq. (11). Equation (11) gives a complete description of the crossover between two characteristic regimes mentioned at the beginning (see Fig. 1(b)) [32]. It also includes small contributions of the suppressed intravalley Cooperons, $\delta_0 = [2e^2/(\pi h)]\ln(\tau_\varphi\tau_*/[\tau(\tau_* + \tau_\varphi)])$ and $\delta(B) = -[2e^2\rho^2/(\pi h)]F[B/(B_\varphi + B_*)]$, where $B_* = \hbar c/(4De\tau_*)$. This permits us to account for a possible difference between the warping time τ_w and the transport time τ. According to Eq. (11) WL MR in bilayer graphene sheet disappears as soon as τ_i exceeds τ_φ, whereas in structures with $\tau_\varphi > \tau_\mathrm{i}$, the result Eq. (11) predicts the WL behavior, as observed

in [34]. Such WL MR is saturated at a magnetic field determined by the intervalley scattering time, instead of the transport time as in usual conductors, which provides the possibility to measure $\tau_{\rm i}$ directly.

4. Conclusions: the effect of edges in nanoribbons

Specifically in graphene, $\mathbf{p} \to -\mathbf{p}$ asymmetry of the electron dispersion (trigonal warping) in each of its valleys, weak disorder in bonds (due to ripples on a graphene sheet), and a finite concentration of dislocation/antidislocation pairs lead to unusual behavior of interference effects in electronic transport. Without intervalley scattering, these effects destroy the manifestation of chirality in the localization properties and the very WL effect itself. Intervalley scattering tends to restore weak localization. This behavior is universal for monolayer and bilayer graphene, despite the fact that electrons in these two materials have different chiralities and can be attributed different Berry phases: π in monolayer, 2π in bilayer [3,5]. This suggests that a suppressed weak localization magnetoresistance and its sensitivity to intervalley scattering are specific to all ultrathin graphitic films independently of their morphology [35] and are determined by the lower (trigonal) symmetry group of the wavevector $\mathbf{K}$ in the corner of the hexagonal Brillouin zone of a honeycomb crystal.

The influence of intervalley scattering on the WL behavior determines a typically negative (WL) MR in graphene nanoribbons. Indeed, in a narrow ribbon of graphene, monolayer or bilayer, with the transverse diffusion time $L_\perp^2/D \ll \tau_{\rm i}, \tau_*, \tau_\varphi$, the sample edges determine strong intervalley scattering rate [36]. Thus, when solving Cooperon equations in a wire, we estimate $\Gamma_0^l \sim \pi^2 D/L_\perp^2$ for the pseudospin triplet, whereas the singlet C_0^0 remains gapless. This yields negative MR persistent over the field range $B < 2\pi B_\perp$, where $B_\perp \equiv \hbar c/eL_\perp^2$:

$$\frac{\Delta\rho_{\rm wire}\,(B)}{\rho^2} = \frac{2e^2 L_\varphi}{h}\left[\frac{1}{\sqrt{1+\frac{1}{3}B^2/B_\varphi B_\perp}} - 1\right]. \qquad (19)$$

The results of Eqs. (10,11,16) and (19) give a complete description of the WL effect in graphene. They describe how the WL magnetoresistance reflects the degree of valley symmetry breaking in the systems and agree with the recent measurements [16,34].

This project has been funded by Lancaster-EPSRC Portfolio Partnership grant EP/C511743 and was completed during the MPI PKS Seminar "Dynamics and Relaxation in Complex Quantum and Classical Systems and Nanostructures."

References

[1] D. DiVincenzo, E. Mele, Phys. Rev. B 29 (1984) 1685.
[2] G.W. Semenoff, Phys. Rev. Lett. 53 (1984) 2449.
[3] F.D.M. Haldane, Phys. Rev. Lett. 61 (1988) 2015;
Y. Zheng, T. Ando, Phys. Rev. B 65 (2002) 245420;
N.M.R. Peres, F. Guinea, A.H. Castro Neto, Phys. Rev. B 73, (2006) 125411;
A.H. Castro Neto, F. Guinea, N.M.R. Peres, Phys. Rev. B 73 (2006) 205408.
[4] T. Ando, T. Nakanishi, R. Saito, J. Phys. Soc. Japan 67 (1998) 2857.
[5] E. McCann, V.I. Fal'ko, Phys. Rev. Lett. 96 (2006) 086805;
J. Nilsson *et al.*, Phys. Rev. B 73 (2006) 214418;
F. Guinea, A.H. Castro Neto, N.M.R. Peres, Phys. Rev. B 73 (2006) 245426;
M. Koshino, T. Ando, Phys. Rev. B 73 (2006) 245403;
B. Partoens, F.M. Peeters, Phys. Rev. B 74 (2006) 075404.
[6] K.S. Novoselov *et al.*, Science 306 (2004) 666.
[7] K.S. Novoselov *et al.*, Nature 438 (2005) 197.
[8] Y. Zhang *et al.*, Phys. Rev. Lett. 94 (2005) 176803;
Y. Zhang *et al.*, Nature 438 (2005) 201.
[9] K.S. Novoselov *et al.*, Nature Physics 2 (2006) 177.
[10] H. Suzuura, T. Ando, Phys. Rev. Lett. 89 (2002) 266603.
[11] D.V. Khveshchenko, Phys. Rev. Lett. 97 (2006) 036802.
[12] S. Hikami, A.I. Larkin, Y. Nagaoka, Prog. Theor. Phys. 63 (1980) 707;
B.L. Al'tshuler *et al.*, Sov. Phys. JETP **54**, (1981) 411 [Zh. Eksp. Teor. Fiz. 81 (1981) 768].
[13] B.L. Altshuler, D. Khmel'nitzkii, A.I. Larkin, P.A. Lee, Phys. Rev. B 22 (1980) 5142.
[14] E. McCann *et al.*, Phys. Rev. Lett. 97 (2006) 146805.
[15] K. Kechedzhi *et al.*, cond-mat/0701690.
[16] S.V. Morozov *et al.*, Phys. Rev. Lett. 97 016801 (2006).
[17] A.F. Morpurgo, F. Guinea, Phys. Rev. Lett. 97 (2006) 196804.
[18] S.V. Iordanskii, A.E. Koshelev, JETP Lett. 41 (1985) 574.
[19] A.W.W. Ludwig, M.P.A. Fisher, R. Shankar, G. Grinstein, Phys. Rev. B 50 (1994) 7526.
[20] I.L Aleiner and K.B. Efetov, Phys. Rev. Lett. 97 (2006) 236801.
[21] K. Ziegler, Phys. Rev. Lett. 97 (2006) 266802.
[22] P.M. Ostrovsky, I.V. Gorny, A.D. Mirlin, Phys. Rev. B 74 (2006) 235443.
[23] V. Cheianov, V.I. Fal'ko, Phys. Rev. B 74 (2006) 041403.
[24] Corners of the hexagonal Brilloin zone are $\mathbf{K}_\pm = \pm(\frac{2}{3}ha^{-1}, 0)$.
[25] P.R. Wallace, Phys. Rev. 71 (1947) 622;
J.C. Slonczewski, P.R. Weiss, Phys. Rev. 109 (1958) 272.
[26] For the monolayer, time reversal of an operator $\hat{W}$ is described by $(\Pi_x \otimes \sigma_x)\hat{W}^*(\Pi_x \otimes \sigma_x)$. For the bilayer, time reversal is given by $\Pi_x \otimes \sigma_x \hat{W}^* \Pi_x \otimes \sigma_x$.
[27] This effect is similar to the recent observation that an in-plane magnetic field induces asymmetry in semiconductor heterostructures and, thus, suppresses the WL effect:
V. Fal'ko, T. Jungwirth, Phys. Rev. B 65 (2002) 081306;
D. Zumbuhl *et al*, Phys. Rev. B 69 (2004) 121305.
[28] The group U_4 can be described using 16 generators $\hat{\mathrm{I}}, \Sigma_s, \Lambda_l, \Sigma_s\Lambda_l,\ s,l = x,y,x$.
[29] E. McCann, V. Fal'ko, Phys. Rev. B 71 (2005) 085415;
N. Peres, F. Guinea, A. Castro Neto, Phys. Rev. B 73 (2006) 125411;
N.H. Shon, T. Ando, J. Phys. Soc. Jpn 67 (1998) 2421;
[30] M. Foster, A. Ludwig, Phys. Rev. B 73 (2006) 155104.
[31] We use pseudospin as a quantum number to classify Cooperons because of the hidden SU_2^Λ symmetry of the dominant part of the free-electron and disorder Hamiltonian.
[32] In this calculation we take into account double spin degeneracy.
[33] M.S. Dresselhaus, G. Dresselhaus, Adv. Phys. 51 (2002) 1;
R.C. Tatar, S. Rabii, Phys. Rev. B 25 (1982) 4126;
J.-C. Charlier, X. Gonze, J.-P. Michenaud, Phys. Rev. B 43 (1991) 4579.
[34] R.V. Gorbachev *et al.*, cond-mat/0701686.
[35] X. Wu *et al.*, cond-mat/0611339.
[36] E. McCann, V.I. Fal'ko, J. Phys. Cond. Matt. 16 (2004) 2371.